Multifunctional high-performance 10-J level laser system

Yujie Peng (彭宇杰)[1,2*], Jiangfeng Wang (王江峰)[1], Zhixiang Zhang (张志祥)[1], Dajie huang (黄大杰)[1], Wei Fan (范 薇)[1], and Xuechun Li (李学春)[1]**

[1]*Shanghai Institute of Optics and Fine Mechanics, Chinese Academy of Sciences, Shanghai 201800, China*

[2]*University of Chinese Academy of Sciences, Beijing 100049, China*

[*]*Corresponding author: yjpeng@siom.ac.cn;* [**]*corresponding author: lixuechun@siom.ac.cn*

Received December 17, 2013; accepted February 12, 2014; posted online April 4, 2014

In this letter, we report a multifunctional high-performance Nd:glass laser system. Laser pulses from an all-fiber front end are first amplified by a regenerative amplifier to 10 mJ level, and then further amplified in a four-pass amplifier. The laser system can provide 10.3-J, 3-ns laser pulses at 1053-nm wavelength. The shot-to-shot energy stability is better than 1.5% (RMS). The output laser beam is near diffraction limit. Binary amplitude masks are used to maintain a flat top near-field profile with a 71% fill factor. After the frequency conversion process, 7 and 5.5 J pulses at 526.5 and 351 nm are obtained, respectively.

OCIS codes: 140.3280, 140.3580, 140.3538.

doi: 10.3788/COL201412.041402.

The primary requirement of most laser systems is the ability to generate high energy pulses with specific spatial and temporal shapes[1]. High-power lasers are typically achieved using power oscillators[2,3] or by master-oscillator power amplifiers (MOPA)[4−6]. For MOPA systems, the front end and power amplifier can be separated. By taking advantage of its configuration, the temporal waveform, spatial shape, and spectrum of the laser beam can be controlled easily.

Earlier laser systems are designed with single-pass multi-stage amplifier chains[7,8]. This design is characterized by numerous amplifiers and telescopes with poor extraction efficiencies and high costs. Studies regarding multi-pass amplifiers (MPA), which could substantially provide higher output energy at a low cost, began in the 1980s[9,10]. The multi-pass architecture only requires the largest final amplifiers and uses several earlier passes through that amplifier instead of initial several-stage amplifiers in single-pass architecture. Thus, the storage extraction efficiency is significantly higher[11]. Most of the newly built laser systems have this structure, whether small-scale experimental systems, such as laser systems[12−14], or large-scale inertial confinement facilities (ICF), such as the National Ignition Facility[15] in the USA and the Laser MegaJoule[16] in France.

The 10-J level laser sources with controllable temporal and spatial distribution are very important for high-power and high-energy laser systems. The main power amplifiers of high-power laser systems always require a multi-joule laser pulse injection with high stability and good beam qualities. Moreover, the optical properties of the injection laser pulse, such as the temporal waveform, spatial distribution, spectral width, and polarization state, could be controlled as needed[17,18]. In addition, the harmonic waves of 10-J level laser sources after frequency conversion can be used as pump laser for optical parametric amplification or for studies regarding optical element damage induced by 3ω laser.

In this letter, a multifunctional high-performance 10-J level laser system based on a four-pass MOPA structure is demonstrated. A >10 J laser pulse at 1053 nm (1ω) is obtained with 3-ns duration. The shot-to-shot energy stability is 1.5% (RMS). The system delivers a nearly diffraction-limited performance, and the near-field of the output laser beam has a near-flat top profile with a 71% fill factor. The laser system can also provide harmonic pulses with 7 J at 526.5 nm (2ω) and 5.5 J at 351 nm (3ω). The laser system can be used not only as the preamplifier of an ICF, but also in other applications, such as studies in optical element damage induced by 3ω laser.

The laser system described in this paper consists of three major components, namely, a master oscillator (MOR), a regenerative amplifier, and an MPA, as shown in Fig. 1.

The MOR for this laser system is similar to that of the Sheng Guang II (SG II) seed laser module[19]. A ∼10-mW single longitudinal mode fiber laser with 1053-nm wavelength is injected into an acousto-optic modulator that can chop the laser pulse into 150-ns width. Then this 150-ns pulse is amplified by an ytterbium-doped fiber amplifier (YDFA). The output pulse of YDFA1 is frequency modulated by a phase modulator to suppress simulated Brillouin scattering (SBS) and protect large-aperture optical elements. The laser is injected into an amplitude modulator driven by an aperture-coupled strip line[20]. The pulse duration can be tuned between 0.1 to 5 ns, and can be adjusted to the desired pulse shape. Furthermore, the temporally shaped pulse is amplified to ~ 1 nJ by YDFA2. The isolators in MOR are used to isolate the backward-propagating lasers, and the filters are used to filter the lasers whose spectra are far from 1053 nm. All of the devices are synchronized by a digital delay pulse generator (SRS, DG645) at a repetition frequency of 1 Hz.

The regenerative amplifier in this laser system consists of a diode-pumped, neodymium-doped phosphate glass rod (N3122) and a folded 540-cm-long cavity. The cavity is designed for working at a stable location, and is composed of two concave high-reflection (HR) end mirrors and an intracavity convex lens. The diode side-pumped laser head provides a single-pass small signal gain of ~ 1.7. The Pockels cell (FastPulse 5046E) in

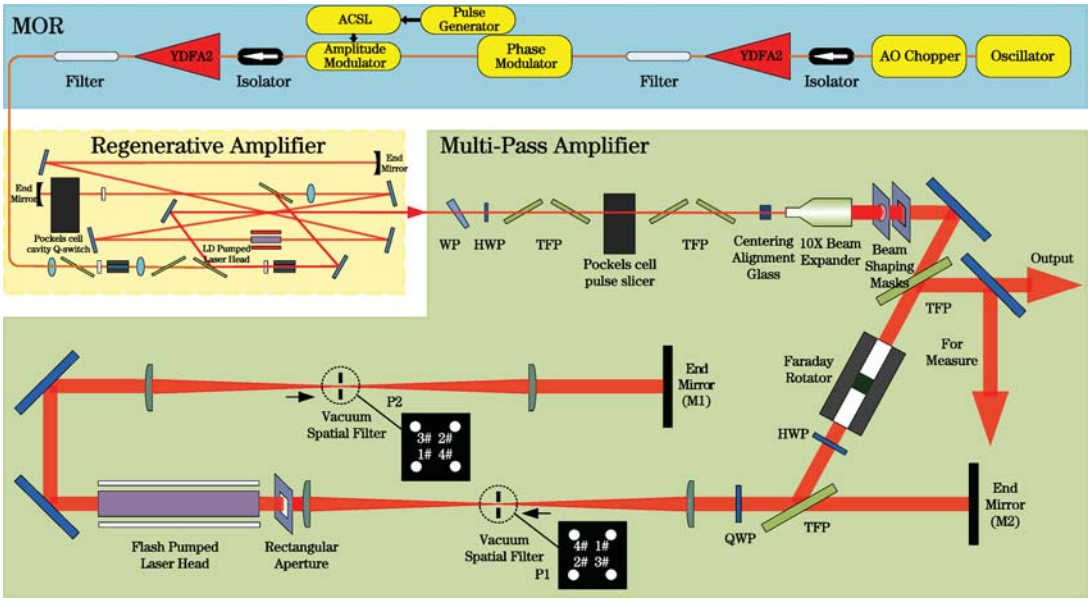

Fig. 1. Schematic of the laser system.

the cavity is used to switch and control laser pulse cycling and ejecting. After approximately 50 round trips, a ~12-mJ amplified pulse is switched out with 0.5% (RMS) long-term stability at a repetition frequency of 1 Hz.

The MPA follows the regenerative amplifier. A wedge plate is used for beam sampling to determine the performance of the regenerative amplifier. A half wave plate (HWP) and two thin film polarizers (TFP) are used to adjust the pulse energy injected into the MPA. The laser pulse passes through a Pockels cell pulse slicer (electro-optical time gate) to clean up the residual prepulse and post-pulse power leakage up to an extinction level near 10,000:1. The off-track light path is adjusted with a centering alignment glass, which is 30-mm thick. The spot size of the laser beam is expanded from 3 to 30 mm by a 10X beam expander. The expanded beam is shaped by two binary amplitude masks. The first is optionally introduced to compensate for the non-uniform spatial gain profile in the MPA. The second binary amplitude mask can shape the laser beam into a square with a profile of 18×18 (mm). The MPA is designed as a four-pass structure that is composed of two end mirrors, a laser amplifier head, a quarter wave plate (QWP), and two vacuum spatial filters (VSF). Each VSF contains a four-element pinhole array, such that each of the four passes is angularly multiplexed. The second binary amplitude mask becomes the reference plane for the relay imaging. The reference plane is relay imaged into the center of the rod, and then onto M1, back to the center of the rod, and then onto M2, and back again. The QWP enables us to select between two-pass or four-pass amplification. We only discuss the four-pass operation in this paper. The MPA optical components are carefully arranged to avoid ghost reflections.

The amplifier head used in the MPA is a flash lamp-pumped Nd:glass rod with 32-mm diameter and 360-mm length. To miniaturize the amplifier head (160×160×450 (mm), 12 flash lamps and the rod are steeped in the cooling water, as shown in Fig. 2.

The amplifier head used in the experiment is described above. To miniaturize the size and structure of the amplifier head, the Nd:glass rod is symmetrically and closely surrounded by 12 flash lamps. The gain distribution of the rod would not be uniform because of the structure of the amplifier head. The voltage supplied to the flash lamps is adjusted near 8.0 kV, and we measure the one-dimensional gain distribution of the amplifier head. The small signal gain G_0 of the different positions is shown in Fig. 3.

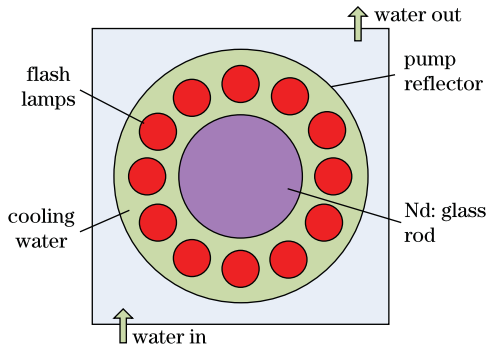

Fig. 2. Structural diagram of the amplifier head in the MPA.

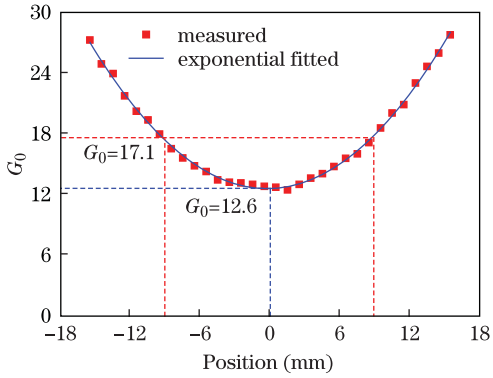

Fig. 3. Small signal gain distribution in the amplifier head.

With a small signal gain from a high-signal pass of the amplifier head, the weak residual reflection will lead to parasitic oscillations. The laser system will be useless as an amplifier until the MPA can be prevented from becoming an oscillator. Figure 4 shows the parasitic oscillation path in the MPA. The net gain of this path is $G_{\rm net} = \frac{G_0^4 T_{4-\rm pass} R_{\rm glint}}{P_{\rm contrast}}$, where $T_{4-\rm pass}$ is the four-pass transmittance of the MPA cavity, $R_{\rm glint}$is the reflectivity of the AR coating on L1, and $P_{\rm contrast}$ is the polarization contrast of the QWP and TFP. The static transmittance of the four-pass amplifier is 65%. The QWP and cavity TFP provide a polarization contrast of 1500:1. Standard AR coating can provide 99.5% transmittance. Therefore, $G_0 < \sqrt[4]{\frac{P_{\rm contrast}}{T_{4-\rm pass} R_{\rm glint}}} = 26$ is required to suppress parasitic oscillation. For the 18×18 (mm) laser beam, the highest gain is about 23 at the four corners of the beam. Parasitic oscillations occur at the edge of the rod and not in the laser beam area. A 22×22 (mm) square aperture is introduced to eliminate the parasitic oscillations caused by the high gain.

The gain distribution of the amplifier head is basically symmetrical. For the 18×18 (mm) laser beam, the ratio of the small signal gain between the center and the edge is about 1.35. Thus, the first binary amplitude mask is optionally designed to compensate for spatial non-uniform gain in the MPA. Based on the description above, the precompensation shaping mask is designed as shown in Fig. 5. The transmittance of the position 9 mm away from the center is about 30%.

After compensating for the non-uniform gain profile, the amplified laser beam profile is shown in Fig. 6. The near-field of the output beam is near flat top, as can be seen in Fig. 6(a). This finding shows that the precompensation binary amplitude mask is designed at the appropriate level. The fill factor is often used to evaluate the uniformity of the near-field of the laser beam. It can be calculated using $FF = \frac{\int I(x,y)\,{\rm d}x{\rm d}y}{I_{\max} A_{\rm beam}}$. For our MPA output beam, the fill factor of the near-field is 71%. Fig. 6(b) shows the measured and ideal energy concentration rate of the focal spot and far-field profile. The diffraction limit in Fig. 6(b) is the zero-order diffraction spot size of the Fraunhofer diffraction of an ideal 18×18 (mm) beam. The output of the MPA is near the diffraction limit.

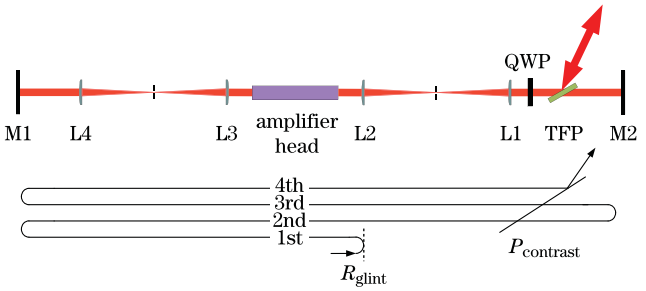

Fig. 4. Schematic of parasitic oscillation path.

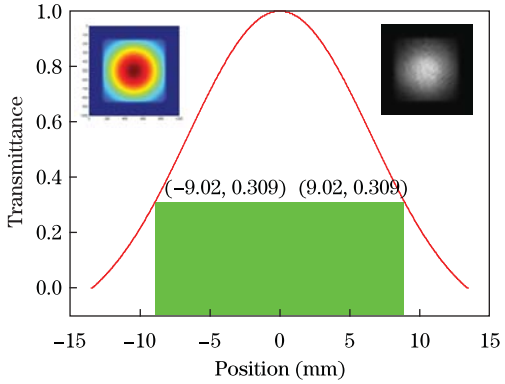

Fig. 5. Designed transmittance of the precompensation shaping mask. The left inset is the designed profile of the MPA-injected laser beam and the right inset is the measured profile.

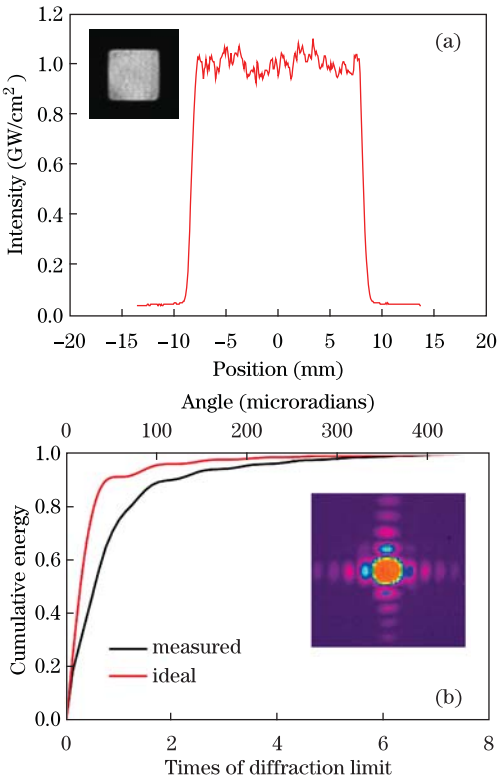

Fig. 6. Near-field beam profile and far-field energy concentration rate of the output beam. (a) One-dimensional intensity distribution of the output laser beam. The inset displays the profile of the near-field; (b) measured and ideal energy concentration rate curve of the focal spot. The inset displays the profile of the far field.

The energy injected into the four-pass amplifier can be adjusted by rotating the HWP following the regenerative amplifier. Figure 7 shows the measured and calculated output energy for the four-pass amplifier. To simplify the calculation process, we assume that the distributions of the spatial intensity of the input laser beam and small signal gain are uniform while we calculate the output energy of the MPA in theory. We also assume that the transmission of each pass is equal. Therefore, in the case of a small signal injection, the measured output energies of the MPA fit well with the calculated curve. However, with the increase in injection, the gain saturation effect limits the output energy of the amplifier, which leads to a deviation between the measured energy and the predicted energy, as shown in Fig. 7. Output energy of 10.3 J is obtained with 1.0-mJ input. The total gain of the four-pass amplifier is more than 10,000. We limit

the output laser pulse energy at this value to reduce the risk of damage to the optical element coating. With a number of operations, the shot-to-shot energy stability is 1.5% (RMS).

In the case of the 10-J output of the MPA, the temporal waveform of the amplified laser pulse is shown in Fig. 8, which approximates the flat top with a nanosecond duration.

The frequency conversion of the 10-J level output laser pulse is demonstrated with two KDP crystals, as shown in Fig. 9(a). The second harmonic generation (SHG) process employs a KDP crystal using type I phase matching and the third harmonic generation (THG) process employs another KDP crystal using the type II phase matching. Up to 7-J second harmonic laser pulse at 526.5 nm and 5.5 J third harmonic at 351 nm are obtained. These results can be used in studies concerning optical element damage. Figure 9(b) shows the near-field beam profile of the 3ω laser beam. The spots and annuluses

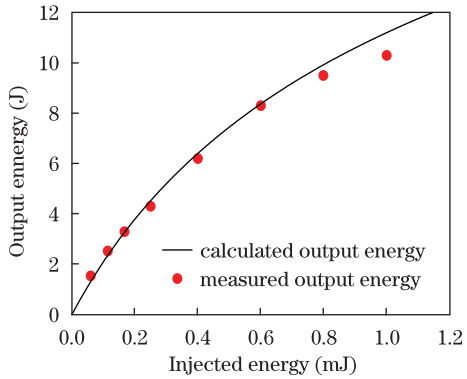

Fig. 7. (Color online) Calculated and measured output energy plotted against injected energy. The solid black line is the calculated output energy using the Frantz-Nodvik model[21] and the red dots are the measured output energy.

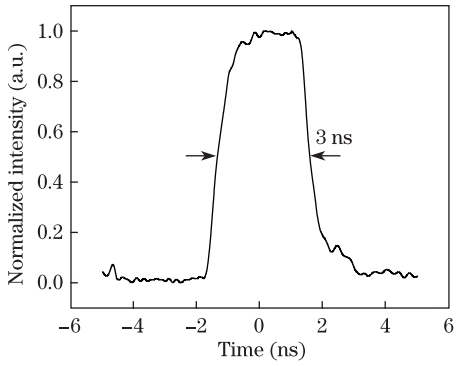

Fig. 8. Temporal waveform of the MPA output laser pulse.

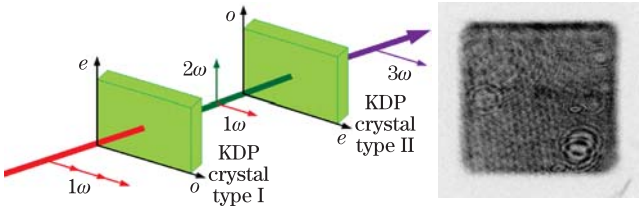

Fig. 9. Frequency conversion process of the MPA output laser. (a) Schematic of the SHG and THG processes; (b) near-field profile of the 3ω laser beam.

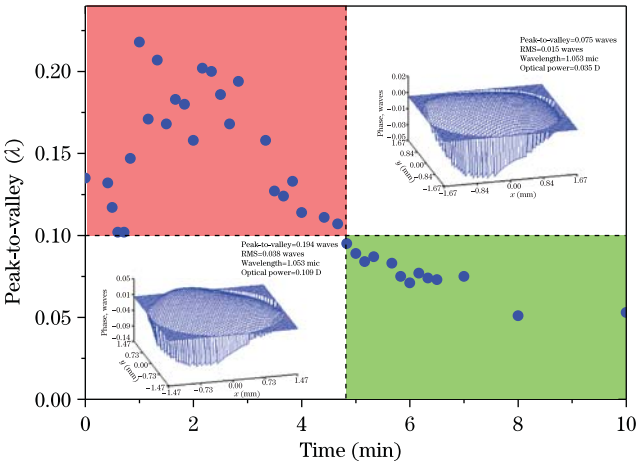

Fig. 10. Measured wavefront distortion (peak-to-valley) after one shot along with the cooling time. The dots are the wavefront distortion peak-to-valley at different time. The lower left inset is the wavefront profile 3 min after the shot and the upper right inset is the wavefront profile 6 min after the shot.

are caused by the dust on the CCD window glass surface. Moreover, the thick modulation is caused by the knife lines while the KDP crystals are cutting.

The MPA system should only operate once per 10 min because of the heat accumulation of the Nd:glass rod. The temperature gradient in the rod may lead to thermally induced depolarization and wavefront distortion.

After one shot, we measure the wavefront distortion of the Nd:glass rod using a Hartmann Shack sensor, which is shown as Fig. 10. The maximum wavefront distortion is located at about 0.22λ. As the laser rod cools, the wavefront distortion decreases. After about 5 min, the distortion recovers to the 0.1λ level, which is slightly adequate for a next shot. Therefore, the miniaturized amplifier head used in our MPA can support a higher operation frequency.

The laser system can operate once per 5 min or even for a shorter time by compensating for the thermally induced depolarization and wavefront distortion[21]. Further studies have been conducted and will be reported in the near future.

In conclusion, we demonstrate a Nd:glass laser system consisting of a master oscillator, a regenerative amplifier, and a four-pass amplifier. In the present work, a 10.3-J laser pulse at 1053-nm (1ω) is obtained with 1.5% (RMS) shot-to-shot fluctuation. By using two shaping masks, a near-diffraction limit flat top laser beam with 71% fill factor is obtained. The laser system can provide harmonic pulses with 7 J at 526.5 nm (2ω) and 5.5 J at 351 nm (3ω). Finally, the possibility of higher frequency operation is discussed. We will increase the repetition rate of the laser system in our future work by compensating for thermally induced depolarization.

References

1. S. E. Bodner, A. J. Schmitt, and J. D. Sethian, High Power Laser Sci. Eng. **1**, 2 (2013).
2. Z. Zhang, Q. Liu, and M. Gong, Laser Phys. Lett. **10**, 035002 (2013).
3. Y. Sun, H. Zhang, Q. Liu, L. Huang, Y. Wang, and M. Gong, Laser Phys. Lett. **7**, 722 (2010).

4. J. Honig, J. Halpin, D. Browning, J. Crane, R. Hackel, M. Henesian, J. Peterson, D. Ravizza, T. Wennberg, H. Rieger, and J. Marciante, Appl. Opt. **46**, 3269 (2007).
5. D. W. Noom, S. Witte, J. Morgenweg, R. K. Altmann, and K. S. Eikema, Opt. Lett. **38**, 3021 (2013).
6. C. B. Dane, L. E. Zapata, W. A. Neuman, M. A. Norton, and L. A. Hackel. IEEE J. Quantum Electron. **31**, 148 (1995).
7. W. W. Simmons, D. R. Speck, and J. T. Hunt. Appl. Opt. **17**, 999 (1978).
8. J. T. Hunt and D. R. Speck, Opt. Eng. **28**, 284461 (1989).
9. J. E. Murray, D. C. Downs, J. T. Hunt, G. L. Hermes, and W. E. Warren, Appl. Opt. **20**, 826 (1981).
10. W. H. Lowdermilk and J. E. Murray, IEEE J. Appl. Phys. **51**, 2436 (1980).
11. M. Gong, Z. Sui, Q. Liu, and X. Fu, Appl. Opt. **52**, 394 (2013).
12. A. Bayramian, P. Armstrong, E. Ault, R. Beach, C. Bibeau, J. Caird, R. Campbell, B. Chai, J. Dawson, C. Ebbers, A. Erlandson, Y. Fei, B. Freitas, R. Kent, Z. Liao, T. Ladran, J. Menapace, B. Molander, S. Payne, N. Peterson, M. Randles, K. Schaffers, S. Sutton, J. Tassano, S. Telford, and E. Utterback, Fusion Science and Technol. **52**, 383 (2007).
13. M. Bowers, S. Burkhart, S. Cohen, G. Erbert, J. Heebner, M. Hermann, and D. Jedlovec, Proc. SPIE **6451**, 64511M-1 (2007).
14. J.-C. Chanteloup, H. Yu, G. Bourdet, C. Dambrine, S. Ferre, A. Fulop, S. Le Moal, A. Pichot, G. L. Touze, and Z. Zhao, Proc. SPIE **5707**, 105 (2005).
15. C. A. Haynam, P. J. Wegner, J. M. Auerbach, M. W. Bowers, S. N. Dixit, G. V. Erbert, G. M. Heestand, M. A. Henesian, M. R. Hermann, K. S. Jancaitis, K. R. Manes, C. D. Marshall, N. C. Mehta, J. Menapace, E. Moses, J. R. Murray, M. C. Nostrand, C. D. Orth, R. Patterson, R. A. Sacks, M. J. Shaw, M. Spaeth, S. B. Sutton, W. H. Williams, C. C. Widmayer, R. K. White, S. T. Yang, and B. M. Van Wonterghem, Appl. Opt. **46**, 3276 (2007).
16. J. Ebrardt and J. M. Chaput. J. Phys.: Conf. Ser. **244,** 032017 (2010).
17. Y. Jiang, S. Zhou, R. Wu, J. Li, X. Li, and Z. Lin, Chin. Opt. Lett. **11**, 081404 (2013).
18. P. Zhang, X. Li, Y. Jiang, and G. Li, Chin. Opt. Lett. **10**, 010602 (2012).
19. Y. Gao, Y. Jiang, and X. Li, Chinese J. Lasers **32**, 1619 (2005).
20. M. D. Skeldon, Rev. Sci. Inst. **71**, 3559 (2000).
21. W. Koechner, *Solid-State Laser Engineering* (Springer, Berlin, 2006).